Vol 17 No 5, May 2008
1674-1056/2008/17(05)/1535-10

Chinese Physics B

© 2008 Chin. Phys. Soc.
and IOP Publishing Ltd

A hybrid scheme for computing incompressible two-phase flows

Zhou Jun(周 军), Cai Li(蔡 力)†, and Zhou Feng-Qi(周凤岐)

Institute of the Precision Guidance and Control, Northwestern Polytechnical University, Xi'an 710072, *China*

(Received 11 July 2007; revised manuscript received 21 September 2007)

We propose a hybrid scheme for computations of incompressible two-phase flows. The incompressible constraint has been replaced by a pressure Poisson-like equation and then the pressure is updated by the modified marker and cell method. Meanwhile, the moment equations in the incompressible Navier–Stokes equations are solved by our semi-discrete Hermite central-upwind scheme, and the interface between the two fluids is considered to be continuous and is described implicitly as the 0.5 level set of a smooth function being a smeared out Heaviside function. It is here named the hybrid scheme. Some numerical experiments are successfully carried out, which verify the desired efficiency and accuracy of our hybrid scheme.

Keywords: two-phase flow, incompressible flow, numerical method
PACC: 0270, 4700, 4755K

1. Introduction

Numerical investigations of incompressible two-phase flows are important in fluid mechanics, marine engineering, aeronautics and astronautics. In general, the ability to predict the corresponding phenomena depends on the availability of mathematical models and numerical methodology (see Refs.[1–5] and references therein).

Here we study the dimensionless incompressible Navier–Stokes equations with continue surface tension[6,7] and gravity, i.e.,

$$\nabla \cdot \boldsymbol{U} = 0,$$

$$\begin{aligned} &\frac{\partial \boldsymbol{U}}{\partial t} + (\boldsymbol{U} \cdot \nabla)\boldsymbol{U} \\ &= -\frac{\nabla p}{\rho} + \frac{1}{\rho R_{\mathrm{e}}} \nabla \left[\mu \left(\nabla \boldsymbol{U} + (\nabla \boldsymbol{U})^{\mathrm{T}} \right) \right] \\ &\quad + \frac{1}{F_{\mathrm{r}}^2} \boldsymbol{g} + \frac{1}{\rho W_{\mathrm{e}}} \boldsymbol{F}_v, \end{aligned} \tag{1}$$

here ∇ is the gradient operator, $\boldsymbol{U} = (u, v)^{\mathrm{T}}$ is the velocity field, p is the pressure, $\boldsymbol{g} = (g_x, g_y)^{\mathrm{T}}$ is the vector in the direction of gravitation, $\boldsymbol{F}_v = (F_v^x, F_v^y)^{\mathrm{T}}$ is a volume force induced by the surface tension, ρ and μ are, respectively, the dimensionless density and viscosity, R_{e} is the Reynolds number, F_{r} is the Froude number and W_{e} is the Weber number.

In this paper, we use a level set function ψ to separate the two fluids, i.e.,

$$\psi(\boldsymbol{x}, t) = \begin{cases} > 0.5, \text{ if } \boldsymbol{x} \in \text{ one of the two fluids,} \\ = 0.5, \text{ if } \boldsymbol{x} \in \text{ the surface between the two fluids,} \\ < 0.5, \text{ if } \boldsymbol{x} \in \text{ the other fluid,} \end{cases} \tag{2}$$

and the volume force $\boldsymbol{F}_v$ can be approximated by $\left(-\nabla \cdot \dfrac{\nabla \psi}{|\nabla \psi|}\right) \nabla \psi$. Then we utilize a modified marker and cell method to discretize Eqs.(1) and derive the pressure Poisson-like equation from the divergence free condition of $\boldsymbol{U}$. If the pressure is updated, we propose a semi-discrete Hermite central-upwind scheme to calculate the velocity field $\boldsymbol{U}$ at the new cycle.

†Corresponding author. E-mail: eign@eyou.com

2. Level set method

In this section we give a brief overview of the level set method (for more details refer to Refs.[7–11], and references therein). Level set method was proposed by Osher and Sethian in Ref.[8] as a simple and versatile method for computing and analysing the subsequent propagation of an interface Γ. This method is easy to be implemented in the presence of boundary singularities or topological changes cases. An interface Γ bounds a (perhaps multiply connected) region Ω of one fluid and propagates with the velocity field $\boldsymbol{U}$. The goal is to define a smooth (at least Lipschitz continuous) function φ, in which Γ can be represented as a set where $\varphi(\boldsymbol{x},t)=0$, i.e. $\Gamma(t)=\{\boldsymbol{x}:\varphi(\boldsymbol{x},t)=0\}$. Then the level set function φ has the following properties:

$$\varphi(\boldsymbol{x},t)=\begin{cases}>0, & \text{if } \boldsymbol{x}\in\bar{\Omega},\\ =0, & \text{if } \boldsymbol{x}\in\partial\Omega=\Gamma(t),\\ <0, & \text{if } \boldsymbol{x}\in\Omega.\end{cases} \tag{3}$$

To represent the density and viscosity discontinuities over the interface, the smeared out Heaviside function

$$H(\varphi)=\begin{cases}0, & \text{if } \varphi<-\varepsilon,\\ 0.5\left[1+\varphi/\varepsilon+\sin(\pi\varphi/\varepsilon)\right]/\pi, & \text{if } |\varphi|\le\varepsilon,\\ 1, & \text{if } \varphi>\varepsilon\end{cases} \tag{4}$$

is needed. Let $\psi=H(\varphi)$, $\rho=\rho_1+(\rho_2-\rho_1)\psi$ and $\mu=\mu_1+(\mu_2-\mu_1)\psi$, then ρ and μ varies smoothly over the interface. Here, ε denotes half the thickness of the interface, ρ_1, ρ_2 and μ_1, μ_2 are the dimensionless densities and viscosities of the two fluids, respectively. Now we can define a sharp interface at $\psi=0.5$ or a diffuse interface for $0<\psi<1$.

Thus, the interface is captured at all later time, by merely locating the 0.5 level set of ψ. Meanwhile, the Eulerian motion formulation is obtained by convecting ψ with the velocity field $\boldsymbol{U}$:

$$\frac{\partial\psi}{\partial t}+\boldsymbol{U}\cdot\nabla\psi=0. \tag{5}$$

To make sure that the interface keeps its thickness and sharpness, the conservative reinitialization step in Ref.[7] is imposed.

3. Marker and cell method

The marker and cell method is proposed by Harlow and Welch in Ref.[12] to calculate the time-dependent viscous incompressible fluid with free surface. Up to now, many extensions of this method are produced and applied in the computational fluid dynamics. See, for instance, Ref.[7].

In this section, we also extend the marker and cell method in Refs.[7,12] and derive the pressure Poisson-like equation from the incompressible constraint. Without loss of generality, the time step is $\triangle t$ and the computational domain $[x_{\min},x_{\max}]\times[y_{\min},y_{\max}]$ are uniformly divided into $N_x\times N_y$ cells with the cell sizes $\triangle x=(x_{\max}-x_{\min})/N_x$ and $\triangle y=(y_{\max}-y_{\min})/N_y$.

We discretize the moment equations in the incompressible Navier–Stokes equations (1) via an extended marker and cell method:

$$\begin{aligned}u^{n+1}_{j+1/2,k}&=u^n_{j+1/2,k}+\triangle tG^n_{j+1/2,k}+\triangle t\frac{g_x}{F_r^2}-\frac{\triangle t}{\triangle x}\frac{p^{n+1}_{j+1,k}-p^{n+1}_{j,k}}{\rho^n_{j+1/2,k}},\\ v^{n+1}_{j,k+1/2}&=v^n_{j,k+1/2}+\triangle tH^n_{j,k+1/2}+\triangle t\frac{g_y}{F_r^2}-\frac{\triangle t}{\triangle y}\frac{p^{n+1}_{j,k+1}-p^{n+1}_{j,k}}{\rho^n_{j,k+1/2}},\end{aligned} \tag{6}$$

where

$$\begin{aligned}G^n_{j+1/2,k}&=\left[-uu_x-vu_y+\frac{(2\mu u_x)_x+(\mu(u_y+v_x))_y}{\rho R_{\mathrm{e}}}+\frac{1}{\rho W_{\mathrm{e}}}F^x_v\right]^n_{j+1/2,k},\\ H^n_{j,k+1/2}&=\left[-uv_x-vv_y+\frac{(2\mu v_y)_y+(\mu(u_y+v_x))_x}{\rho R_{\mathrm{e}}}+\frac{1}{\rho W_{\mathrm{e}}}F^y_v\right]^n_{j,k+1/2}.\end{aligned}$$

Here we offer the derivation of the discretization of the flux $H^n_{j,k+1/2}$, while the discretization of the flux $G^n_{j+1/2,k}$ can be obtained in a similar way.

The surface tension $(F^y_v)^n_{j,k+1/2}$ can be approximated by

$$(F_v^y)^n_{j,k+1/2} = 0.5\left[\left(-\nabla\cdot\frac{\nabla\psi}{|\nabla\psi|}\right)^n_{j,k}(\psi_y)^n_{j,k} + \left(-\nabla\cdot\frac{\nabla\psi}{|\nabla\psi|}\right)^n_{j,k+1}(\psi_y)^n_{j,k+1}\right],$$

where

$$\left(\nabla\cdot\frac{\nabla\psi}{|\nabla\psi|}\right)^n_{j,k} = \frac{1}{2\triangle x}\left[\frac{(\psi_x)^n_{j+1,k}}{\sqrt{\left((\psi_x)^n_{j+1,k}\right)^2+\left((\psi_y)^n_{j+1,k}\right)^2}} - \frac{(\psi_x)^n_{j-1,k}}{\sqrt{\left((\psi_x)^n_{j-1,k}\right)^2+\left((\psi_y)^n_{j-1,k}\right)^2}}\right]$$
$$+\frac{1}{2\triangle y}\left[\frac{(\psi_y)^n_{j,k+1}}{\sqrt{\left((\psi_x)^n_{j,k+1}\right)^2+\left((\psi_y)^n_{j,k+1}\right)^2}} - \frac{(\psi_y)^n_{j,k-1}}{\sqrt{\left((\psi_x)^n_{j,k-1}\right)^2+\left((\psi_y)^n_{j,k-1}\right)^2}}\right]$$

with $(\psi_x)^n_{j,k} = \dfrac{\psi^n_{j+1,k}-\psi^n_{j-1,k}}{2\triangle x}$ and $(\psi_y)^n_{j,k} = \dfrac{\psi^n_{j,k+1}-\psi^n_{j,k-1}}{2\triangle y}$. The other terms of $H^n_{j,k+1/2}$ are calculated by

$$(uv_x)^n_{j,k+1/2} = \frac{1}{4}\left(u^n_{j+1/2,k}+u^n_{j-1/2,k}+u^n_{j+1/2,k+1}+u^n_{j-1/2,k+1}\right)\frac{v^n_{j+1/2,k+1/2}-v^n_{j-1/2,k+1/2}}{\triangle x},$$
$$(vv_y)^n_{j,k+1/2} = v^n_{j,k+1/2}\frac{v^n_{j,k+1}-v^n_{j,k}}{\triangle y},$$
$$[(\mu v_y)_y]^n_{j,k+1/2} = \frac{\mu^n_{j,k+1}\left(v^n_{j,k+3/2}-v^n_{j,k+1/2}\right)-\mu^n_{j,k}\left(v^n_{j,k+1/2}-v^n_{j,k-1/2}\right)}{\triangle y^2},$$
$$[(\mu u_y)_x]^n_{j,k+1/2} = \frac{\mu^n_{j+1/2,k+1/2}\left(u^n_{j+1/2,k+1}-u^n_{j+1/2,k}\right)-\mu^n_{j-1/2,k+1/2}\left(u^n_{j-1/2,k+1}-u^n_{j-1/2,k}\right)}{\triangle x\triangle y},$$
$$[(\mu v_x)_x]^n_{j,k+1/2} = \frac{\mu^n_{j+1/2,k+1/2}\left(v^n_{j+1,k+1/2}-v^n_{j,k+1/2}\right)-\mu^n_{j-1/2,k+1/2}\left(v^n_{j,k+1/2}-v^n_{j-1,k+1/2}\right)}{\triangle x^2}.$$

Finally, we require $\boldsymbol{U}$ to be divergence free at any cycle, i.e.,

$$(\nabla\cdot\boldsymbol{U})_{j,k} = \frac{u_{j+1/2,k}-u_{j-1/2,k}}{\triangle x}+\frac{v_{j,k+1/2}-v_{j,k-1/2}}{\triangle y} = 0,$$

and thus we obtain the pressure Poisson-like equation

$$\frac{1}{\triangle x^2}\left(\frac{p^{n+1}_{j+1,k}-p^{n+1}_{j,k}}{\rho^n_{j+1/2,k}}-\frac{p^{n+1}_{j,k}-p^{n+1}_{j-1,k}}{\rho^n_{j-1/2,k}}\right)+\frac{1}{\triangle y^2}\left(\frac{p^{n+1}_{j,k+1}-p^{n+1}_{j,k}}{\rho^n_{j,k+1/2}}-\frac{p^{n+1}_{j,k}-p^{n+1}_{j,k-1}}{\rho^n_{j,k-1/2}}\right)$$
$$= \frac{G^n_{j+1/2,k}-G^n_{j-1/2,k}}{\triangle x}+\frac{H^n_{j,k+1/2}-H^n_{j,k-1/2}}{\triangle y}. \tag{7}$$

4. Semi-discrete Hermite central-upwind scheme

In this section, we deduce the 2D semi-discrete Hermite central-upwind scheme. Without loss of generality, we consider the 2D Hamilton–Jacobi equation

$$\phi_t + H(\phi_x,\phi_y) = 0, \tag{8}$$

subject to the initial data $\phi(x,y,t=0)=\phi_0(x,y)$. We assume that the approximate solution at time t^n, ϕ^n_{jk}, is given and that a continuous piecewise polynomial interpolation, $\tilde{\phi}(x,y,t^n)$, is reconstructed from ϕ^n_{jk}. Here, the time step $\triangle t$ should satisfy $x^n_{j+,k} < x^n_{j+1-,k}$ and $y^n_{j,k+} < y^n_{j,k+1-}$ for all j and k.

At every grid point (x_j,y_k), the maximal one-sided local speeds of propagation in x- and y-directions, $a^{\pm}_{jk}$ and $b^{\pm}_{jk}$, can be estimated by

$$a^+_{jk} = \max_{\tilde{\phi}_x\in I_x,\ \tilde{\phi}_y\in I_y}\left\{H_u(\tilde{\phi}_x(x,y,t^n),\tilde{\phi}_y(x,y,t^n)),0\right\},$$
$$a^-_{jk} = \left|\min_{\tilde{\phi}_x\in I_x,\ \tilde{\phi}_y\in I_y}\left\{H_u(\tilde{\phi}_x(x,y,t^n),\tilde{\phi}_y(x,y,t^n)),0\right\}\right|,$$

$$b_{jk}^{+}=\max_{\tilde{\phi}_x\in I_x,\ \tilde{\phi}_y\in I_y}\left\{H_v(\tilde{\phi}_x(x,y,t^n),\tilde{\phi}_y(x,y,t^n)),0\right\},$$

$$b_{jk}^{-}=\left|\min_{\tilde{\phi}_x\in I_x,\ \tilde{\phi}_y\in I_y}\left\{H_v(\tilde{\phi}_x(x,y,t^n),\tilde{\phi}_y(x,y,t^n)),0\right\}\right|,$$

with $I_x=[\min\{\phi_x^+,\phi_x^-\},\max\{\phi_x^+,\phi_x^-\}]$ and $I_y=[\min\{\phi_y^+,\phi_y^-\},\max\{\phi_y^+,\phi_y^-\}]$. Here $\phi_x^{\pm}=\tilde{\phi}_x(x_j\pm 0,y_k,t^n)$ and $\phi_y^{\pm}=\tilde{\phi}_y(x_j,y_k\pm 0,t^n)$.

The reconstructions $\tilde{\phi}(x,y,t^n)$ at the grid points are then evolved around $(x_{j\pm}^n,y_{k\pm}^n)=(x_j\pm a_{jk}^{\pm}\triangle t,y_k\pm b_{jk}^{\pm}\triangle t)$ according to the Hamilton–Jacobi equation (8). We denote $\tilde{\phi}_{j\pm,k\pm}^n=\tilde{\phi}(x_{\pm}^n,y_{\pm}^n,t^n)$ and use the Taylor expansion in space to compute the values of $\tilde{\phi}_{j\pm,k\pm}^n$ as follows:

$$\begin{aligned}\tilde{\phi}_{j\pm,k\pm}^n&=\phi_{jk}^n\pm\triangle ta_{jk}^{\pm}\phi_x^{\pm}\pm\triangle tb_{jk}^{\pm}\phi_y^{\pm}+\mathcal{O}(\triangle t^2)\\&=\phi_{jk}^n\pm\triangle ta_{jk}^{\pm}\tilde{\phi}_x(x_j\pm 0,y_k,t^n)\\&\quad\pm\triangle tb_{jk}^{\pm}\tilde{\phi}_y(x_j,y_k\pm 0,t^n)+\mathcal{O}(\triangle t^2).\end{aligned}\tag{9}$$

At the same time, we use the Taylor expansion in time to approximate the intermediate values at the next time level $t=t^{n+1}$

$$\begin{aligned}&\phi_{j\pm,k\pm}^n\\&=\tilde{\phi}_{j\pm,k\pm}^n-\triangle tH\left(\tilde{\phi}_x(x_{j\pm}^n,y_{k\pm}^n,t^n),\tilde{\phi}_y(x_{j\pm}^n,y_{k\pm}^n,t^n)\right)\\&\quad+\mathcal{O}(\triangle t^2).\end{aligned}\tag{10}$$

Substituting Eq.(9) in Eq.(10) yields

$$\begin{aligned}&\phi_{j\pm,k\pm}^{n+1}\\&=\phi_{jk}^n\pm\triangle ta_{jk}^{\pm}\tilde{\phi}_x(x_j\pm 0,y_k,t^n)\\&\quad\pm\triangle tb_{jk}^{\pm}\tilde{\phi}_y(x_j,y_k\pm 0,t^n)\\&\quad-\triangle tH\left(\tilde{\phi}_x(x_{j\pm}^n,y_{k\pm}^n,t^n),\tilde{\phi}_y(x_{j\pm}^n,y_{k\pm}^n,t^n)\right)\\&\quad+\mathcal{O}(\triangle t^2).\end{aligned}\tag{11}$$

We now project the intermediate values $\phi_{j\pm,k\pm}^n$ back onto the original grid points. We construct a 1D cubic Hermite interpolation in y-direction at first, i.e.,

$$\begin{aligned}\tilde{\varphi}(x_{j\pm}^n,y,t^{n+1})=&\left[1-\frac{2(y-y_{k-}^n)}{y_{k-}^n-y_{k+}^n}\right]\left(\frac{y-y_{k+}^n}{y_{k-}^n-y_{k+}^n}\right)^2\phi_{j\pm,k-}^{n+1}+\left[1-\frac{2(y-y_{k+}^n)}{y_{k+}^n-y_{k-}^n}\right]\left(\frac{y-y_{k-}^n}{y_{k+}^n-y_{k-}^n}\right)^2\phi_{j\pm,k+}^{n+1}\\&+(y-y_{k-}^n)\left(\frac{y-y_{k+}^n}{y_{k-}^n-y_{k+}^n}\right)^2\phi_y^{+}+(y-y_{k+}^n)\left(\frac{y-y_{k-}^n}{y_{k+}^n-y_{k-}^n}\right)^2\phi_y^{-}.\end{aligned}\tag{12}$$

Next, we use the values $\tilde{\varphi}(x_{j\pm}^n,y,t^{n+1})$ to construct another 1D cubic Hermite interpolation in x-direction

$$\begin{aligned}&\tilde{\varphi}(x,y_k,t^{n+1})\\=&\left[1-\frac{2(x-x_{j-}^n)}{x_{j-}^n-x_{j+}^n}\right]\left(\frac{x-x_{j+}^n}{x_{j-}^n-x_{j+}^n}\right)^2\tilde{\varphi}(x_{j-}^n,y_k,t^{n+1})+\left[1-\frac{2(x-x_{j+}^n)}{x_{j+}^n-x_{j-}^n}\right]\left(\frac{x-x_{j-}^n}{x_{j+}^n-x_{j-}^n}\right)^2\tilde{\varphi}(x_{j+}^n,y_k,t^{n+1})\\&+(x-x_{j-}^n)\left(\frac{x-x_{j+}^n}{x_{j-}^n-x_{j+}^n}\right)^2\phi_x^{+}+(x-x_{j+}^n)\left(\frac{x-x_{j-}^n}{x_{j+}^n-x_{j-}^n}\right)^2\phi_x^{-}+\mathcal{O}(\triangle t^4).\end{aligned}\tag{13}$$

Therefore, the evolved solution at the original grid point (x_j,y_k) at time t^{n+1} is

$$\begin{aligned}\phi_{jk}^{n+1}&=\tilde{\varphi}(x_j,y_k,t^{n+1})\\&=\phi_{jk}^n+\left(1+\frac{2a_{jk}^{+}}{a_{jk}^{-}+a_{jk}^{+}}\right)\left(\frac{a_{jk}^{-}}{a_{jk}^{-}+a_{jk}^{+}}\right)^2\triangle ta_{jk}^{+}\phi_x^{+}-\left(1+\frac{2a_{jk}^{-}}{a_{jk}^{-}+a_{jk}^{+}}\right)\left(\frac{a_{jk}^{+}}{a_{jk}^{-}+a_{jk}^{+}}\right)^2\triangle ta_{jk}^{-}\phi_x^{-}\\&\quad+\left(1+\frac{2b_{jk}^{+}}{b_{jk}^{-}+b_{jk}^{+}}\right)\left(\frac{b_{jk}^{-}}{b_{jk}^{-}+b_{jk}^{+}}\right)^2\triangle tb_{jk}^{+}\phi_y^{+}-\left(1+\frac{2b_{jk}^{-}}{b_{jk}^{-}+b_{jk}^{+}}\right)\left(\frac{b_{jk}^{+}}{b_{k}^{-}+b_{jjk}^{+}}\right)^2\triangle tb_{jk}^{-}\phi_y^{-}\\&\quad+\triangle ta_{jk}^{-}\left(\frac{a_{jk}^{+}}{a_{jk}^{-}+a_{jk}^{+}}\right)^2\phi_x^{+}-\triangle ta_{jk}^{+}\left(\frac{a_{jk}^{-}}{a_{jk}^{-}+a_{jk}^{+}}\right)^2\phi_x^{-}\\&\quad+\triangle tb_{jk}^{-}\left(\frac{b_{jk}^{+}}{b_{jk}^{-}+b_{jk}^{+}}\right)^2\phi_y^{+}-\triangle tb_{jk}^{+}\left(\frac{b_{jk}^{-}}{b_{jk}^{-}+b_{jk}^{+}}\right)^2\phi_y^{-}\\&\quad-\triangle t\left[C_{++}H(\phi_x^{+},\phi_y^{+})+C_{+-}H(\phi_x^{+},\phi_y^{-})+C_{-+}H(\phi_x^{-},\phi_y^{+})+C_{--}H(\phi_x^{-},\phi_y^{-})\right]+\mathcal{O}(\triangle t^2),\end{aligned}\tag{14}$$

where

$$C_{++} = \left(1+\frac{2a^+_{jk}}{a^-_{jk}+a^+_{jk}}\right)\left(\frac{a^-_{jk}}{a^-_{jk}+a^+_{jk}}\right)^2\left(1+\frac{2b^+_{jk}}{b^-_{jk}+b^+_{jk}}\right)\left(\frac{b^-_{jk}}{b^-_{jk}+b^+_{jk}}\right)^2,$$

$$C_{+-} = \left(1+\frac{2a^+_{jk}}{a^-_{jk}+a^+_{jk}}\right)\left(\frac{a^-_{jk}}{a^-_{jk}+a^+_{jk}}\right)^2\left(1+\frac{2b^-_{jk}}{b^-_{jk}+b^+_{jk}}\right)\left(\frac{b^+_{jk}}{b^-_{jk}+b^+_{jk}}\right)^2,$$

$$C_{-+} = \left(1+\frac{2a^-_{jk}}{a^-_{jk}+a^+_{jk}}\right)\left(\frac{a^+_{jk}}{a^-_{jk}+a^+_{jk}}\right)^2\left(1+\frac{2b^+_{jk}}{b^-_{jk}+b^+_{jk}}\right)\left(\frac{b^-_{jk}}{b^-_{jk}+b^+_{jk}}\right)^2,$$

$$C_{--} = \left(1+\frac{2a^-_{jk}}{a^-_{jk}+a^+_{jk}}\right)\left(\frac{a^+_{jk}}{a^-_{jk}+a^+_{jk}}\right)^2\left(1+\frac{2b^-_{jk}}{b^-_{jk}+b^+_{jk}}\right)\left(\frac{b^+_{jk}}{b^-_{jk}+b^+_{jk}}\right)^2.$$

It is the fully-discrete Hermite scheme for 2D Hamilton–Jacobi equation (8).

Let the limit $\triangle t \to 0$ generates a semi-discrete Hermite scheme for 2D Hamilton–Jacobi equation (8):

$$\begin{aligned}\frac{\mathrm{d}}{\mathrm{d}t}\phi_{jk}(t) = {} & \left(1+\frac{2a^+_{jk}}{a^-_{jk}+a^+_{jk}}\right)\left(\frac{a^-_{jk}}{a^-_{jk}+a^+_{jk}}\right)^2 a^+_{jk}\phi^+_x - \left(1+\frac{2a^-_{jk}}{a^-_{jk}+a^+_{jk}}\right)\left(\frac{a^+_{jk}}{a^-_{jk}+a^+_{jk}}\right)^2 a^-_{jk}\phi^-_x \\ & + \left(1+\frac{2b^+_{jk}}{b^-_{jk}+b^+_{jk}}\right)\left(\frac{b^-_{jk}}{b^-_{jk}+b^+_{jk}}\right)^2 b^+_{jk}\phi^+_y - \left(1+\frac{2b^-_{jk}}{b^-_{jk}+b^+_{jk}}\right)\left(\frac{b^+_{jk}}{b^-_{jk}+b^+_{jk}}\right)^2 b^-_{jk}\phi^-_y \\ & + a^-_{jk}\left(\frac{a^+_{jk}}{a^-_{jk}+a^+_{jk}}\right)^2\phi^+_x - a^+_{jk}\left(\frac{a^-_{jk}}{a^-_{jk}+a^+_{jk}}\right)^2\phi^-_x \\ & + b^-_{jk}\left(\frac{b^+_{jk}}{b^-_{jk}+b^+_{jk}}\right)^2\phi^+_y - b^+_{jk}\left(\frac{b^-_{jk}}{b^-_{jk}+b^+_{jk}}\right)^2\phi^-_y \\ & - \left[C_{++}H(\phi^+_x,\phi^+_y) + C_{+-}H(\phi^+_x,\phi^-_y) + C_{-+}H(\phi^-_x,\phi^+_y) + C_{--}H(\phi^-_x,\phi^-_y)\right]. \end{aligned} \tag{15}$$

Using the dimension-by-dimension approach (see, e.g., Ref.[13]), the 2D extensions of the WENO interpolations can be easily obtained and then can be used to calculate the one-side derivatives in Eq.(15). In the following numerical tests, the third-order TVD Runge–Kutta method in Ref.[13] is imposed as the ODE solver to integrate Eq.(15).

Obviously, the semi-discrete Hermite central-upwind scheme (15) can solve the evolving equation (5) directly. To calculate the new velocity field $\boldsymbol{U}$, we use the second-order centred difference approximations to the right hand side of the moment equations in the incompressible Navier–Stokes equations (1), while the advection terms on the left hand side can be discretized by the scheme (15).

5. Algorithm of the hybrid scheme

In this section, we present a complete description of the hybrid algorithm we use in this paper:

1) Choose a level set function at time t, i.e., $\psi(\boldsymbol{x}, t)$, which satisfies the constraint (2);

2) Solve the evolving equation (5) via the semi-discrete Hermite central-upwind scheme (15) and update the level set function;

3) Use the extended marker and cell method in Section 3 to solve the pressure Poisson-like equation (7) and obtain the new pressure at time $t + \triangle t$;

4) Utilize the semi-discrete Hermite central-upwind scheme (15) and the second-order centred difference approximations to obtain the new velocity field $\boldsymbol{U}$ at time $t + \triangle t$;

5) To make sure that the interface keeps its thickness and sharpness, the conservative reinitialization step in Ref.[7] is imposed, and then go to step 2).

6. Numerical examples

We test our hybrid scheme for five different cases: vortex test, shear-layer problem, rising bubble, flow induced by wall adhesion in zero gravity and the liq-

uid sloshing in zero gravity.

6.1. Vortex test

To test our advection scheme, the semi-discrete Hermite central-upwind scheme, on a complicated flow (refer to Ref.[7]), we use the following velocity field, $u = -\sin^2(\pi x)\sin(2\pi y)$ and $v = \sin^2(\pi y)\sin(2\pi x)$, on a unit square. A circle with a radius 0.15 centred at (0.5, 0.75) is imposed as the initial condition. At $t = T$ the flow field is reversed, hence the exact solution at time $t = 2T$ should coincide with the initial condition. The computational domain is discretized by 100×100 cells. We select T as 1 and ε as $0.5\triangle x$. The results are shown in Fig.1. We also perform a long time no-reversed simulations on the 100×100 cells with an initial circle centred at (0.5, 0.65). The solutions at time t ranging from 1 to 4 are described in Fig.2.

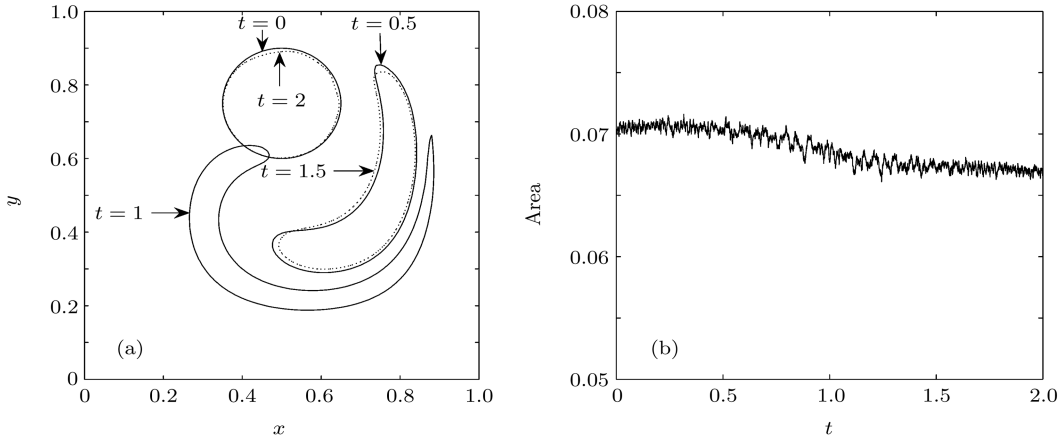


Fig.1. Vortex test: (a) evolving solutions; (b) the area of the vortex.

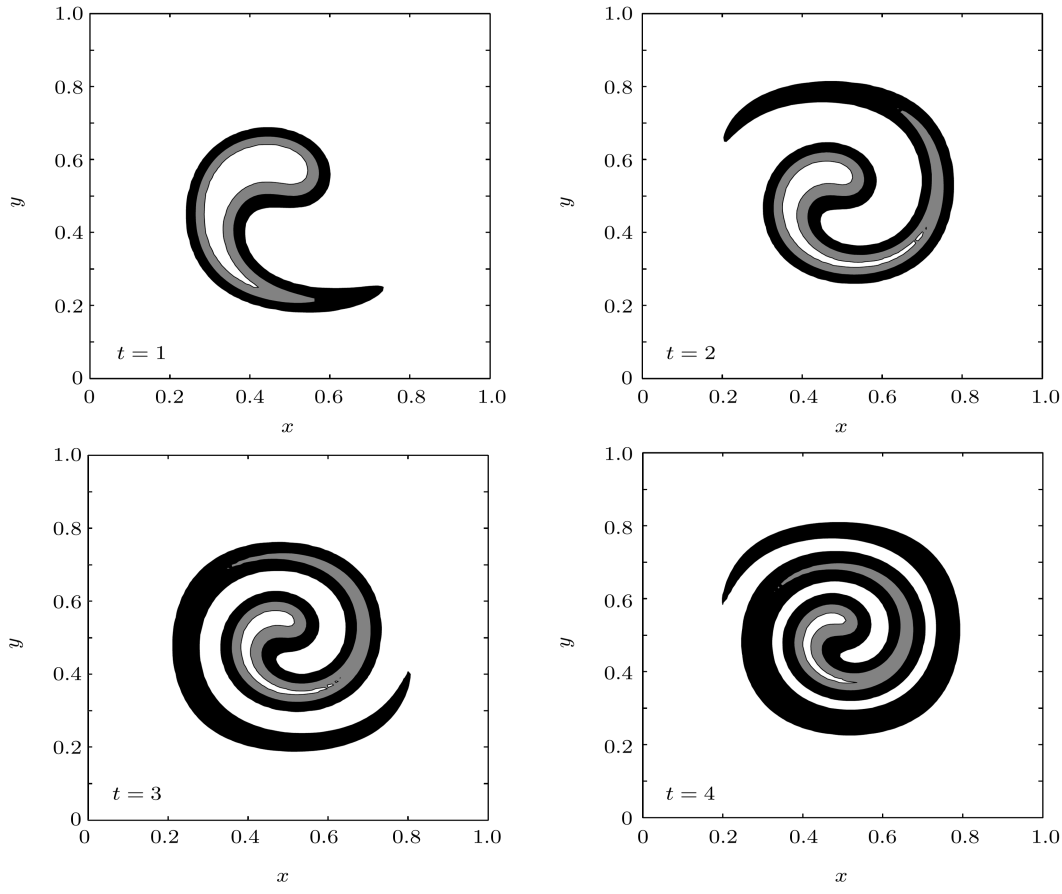


Fig.2. Vortex test: long time simulations.

6.2. Shear-layer problem

The periodic double shear-layer problem in Ref.[14] is simulated to check the efficiency of the extended marker and cell method, given in Section 3. First, we solve the incompressible Euler equations subject to $(2\pi, 2\pi)$-periodic initial data. The numerical results at time $t = 10$ for 60×60 grid cells are described in the left column of Fig.3. For the same conditions, we solve the incompressible Navier–Stokes equations. See the right column of Fig.3. The qualitative results obtained with our method agree with that in Ref.[14].

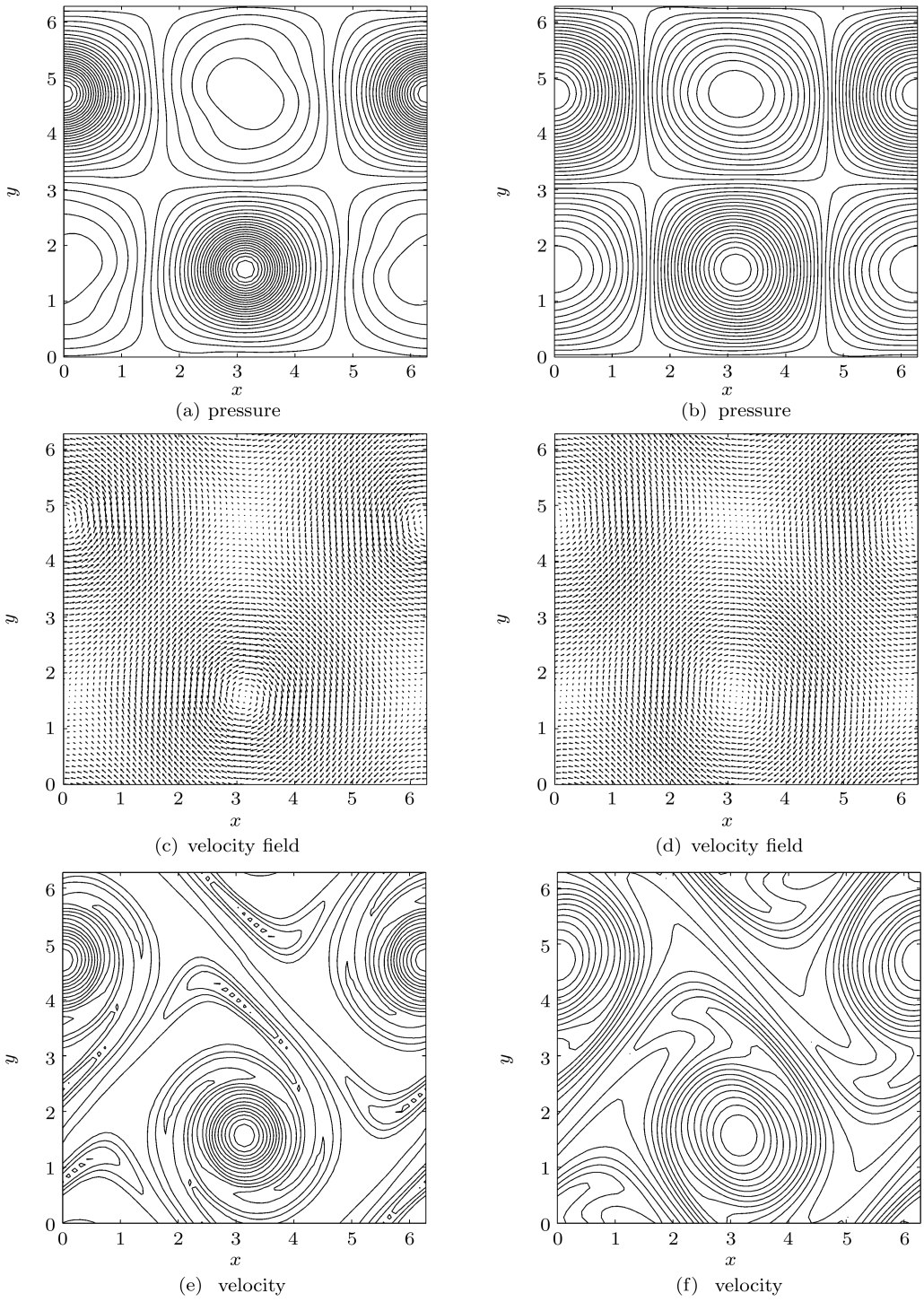


Fig.3. Numerical solutions: (left) results of the incompressible Euler equations; (right) results of the incompressible Navier–Stokes equations.

6.3. Rising bubble

Consider an air bubble in water initially at rest. We select $g_x = 0$, $g_y = -10$, $R_e = 500$, $F_r = 0.45$, $W_e = 0.68$, $\rho_1 = 1$, $\rho_2 = 0.013$, $\mu_1 = 1$ and $\mu_2 = 0.016$ throughout the following numerical tests. Computations are performed in the domain $[0, 2] \times [0, 2]$ with 40×40 grid cells. Results, i.e. the velocity field and the interface of the bubbles, at time $t = 0.263$ are shown in Fig.4(a). We also plot the evolving area of the air bubbles, shown in Fig.4(b).

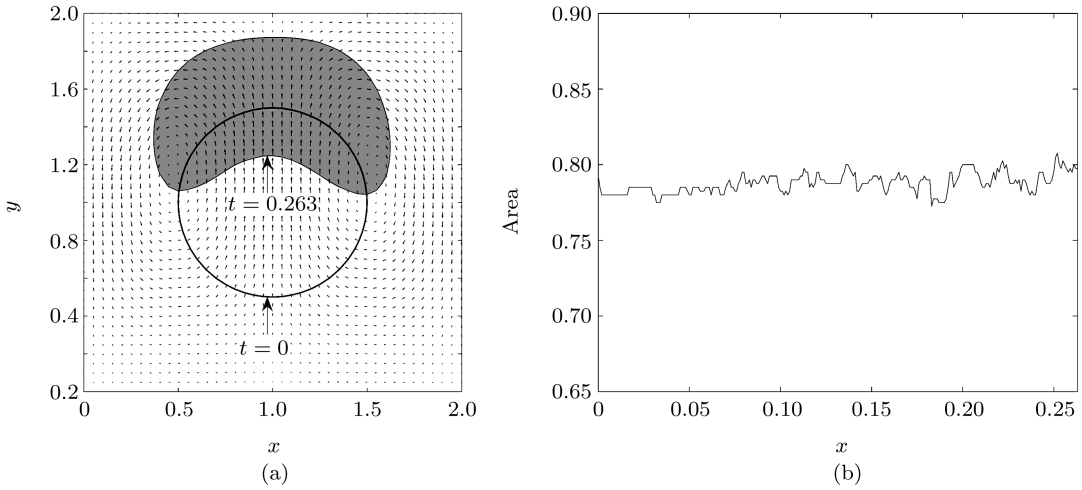


Fig.4. Rising bubble: (a) the velocity field and the interface of the bubbles; (b) the area of the air bubble.

6.4. Flow induced by wall adhesion in zero gravity

As an example of the effects of wall adhesion in zero gravity computed with our hybrid scheme, consider a shallow pool of liquid fuel located at the bottom of a rectangular tank in a satellite. As is known, the gas and the liquid fuel are pressed to store in the tank. Since the pressure is invariable at the initial time, the compressibility of the gas can be omitted. Assume that the liquid interface should arrive at a specified contact angle θ. Two different cases are considered: the contact angle $\theta = \pi/3$ (see Fig.5) and $\theta = 2\pi/3$ (see Fig.6). In Fig.5, we describe the interfaces of the liquid and the velocity fields at time $t = 0.1$ and $t = 0.4$. In Fig.6, we give the stationary interface and the velocity field with the different liquid volumes: 0.3344 and 0.4311. The domain $[0, 1] \times [0, 1]$ is discretized with 30×30 grid cells.

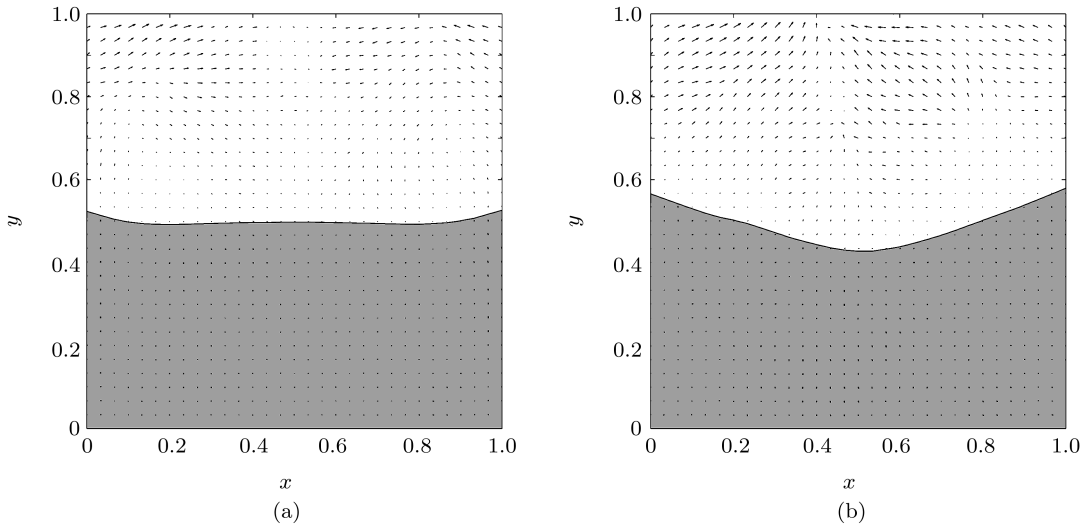


Fig.5. Interfaces with $\theta = \pi/3$ at different times: (a) $t = 0.1$ and (b) $t = 0.4$.

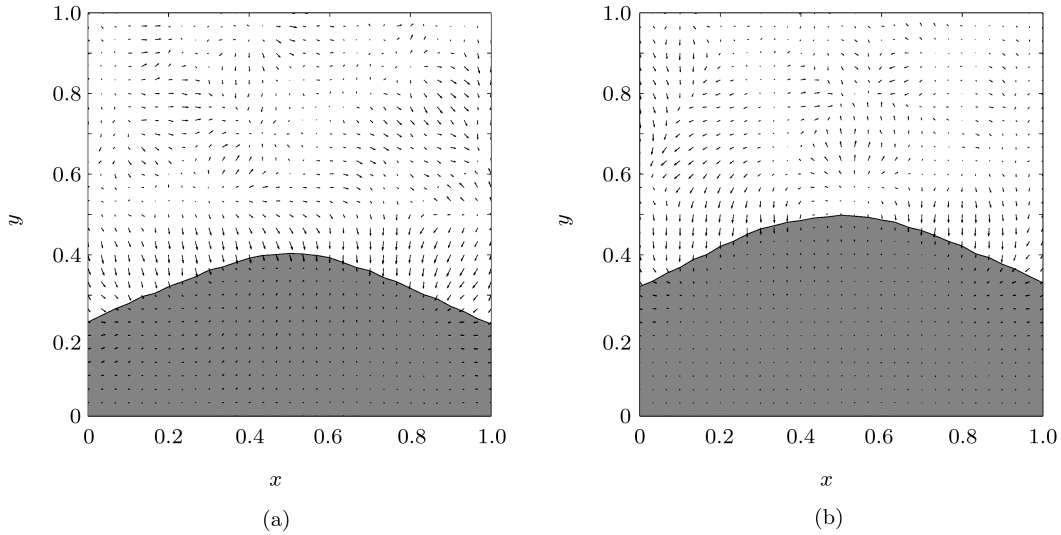


Fig.6. Interfaces with $\theta = 2\pi/3$ and the different liquid volumes: (a) 0.3344 and (b) 0.4311.

6.5. Liquid sloshing in zero gravity

Nonlinear sloshing in zero gravity inside a surging partially filled rectangular tank has been investigated. Likewise, the pressure changes slightly and the compressibility of the gas can be also omitted. The surge motion is given by $\ddot{X}_0 = -X_0\omega_x^2 \sin(\omega_x t)$, where $X_0 = 0.5$ is the maximum horizontal amplitude, $\omega_x = 8\pi$ is the surge frequency, with the contact angle $\theta = \pi/2$. The sloshing surface of the liquid and the corresponding velocity field at time 0.0564 is described in Fig.7(a), while Fig.7(b) shows the results at time $t = 0.071$. Computations are performed in the domain $[0,1] \times [0,1]$ with 30×30 grid cells.

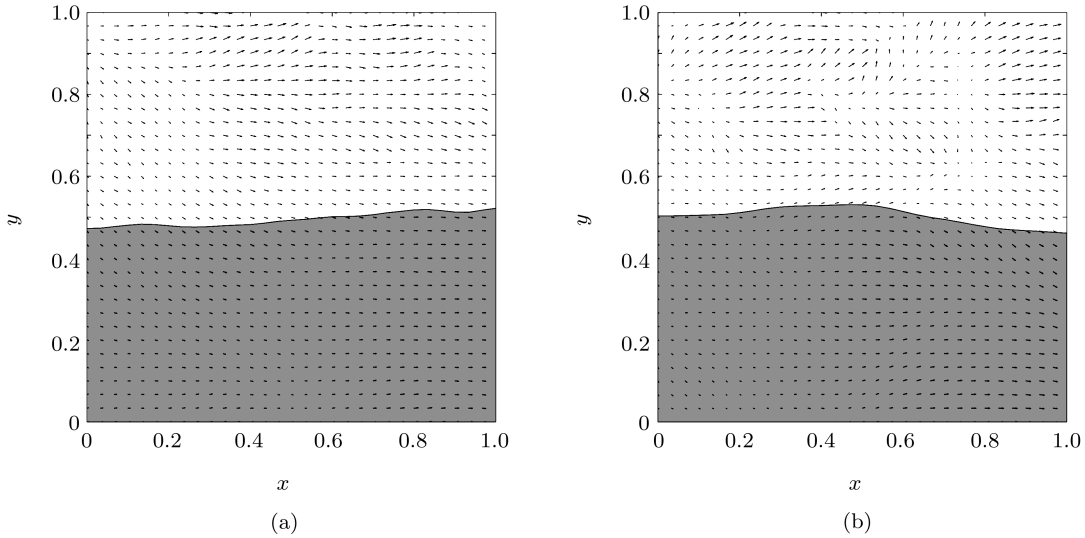


Fig.7. Liquid sloshing at different times: (a) $t = 0.0564$ and (b) $t = 0.071$.

7. Conclusions

A hybrid scheme for computations of incompressible two-phase flows is proposed and the desired efficiency and accuracy of the scheme are verified via some numerical examples. The conservation of the area within the scheme is shown in the vortex test, and the sloshing results in the fully filled tank are discussed in the shear-layer problem. As an example,

the rising bubble is computed to show the results of incompressible two-phase flows in nonzero gravity. In zero gravity case, the flow induced by wall adhesion and the liquid sloshing problems are investigated. We can calculate the stationary interfaces and the velocity fields with the different liquid volumes and contact angles. At the same time, the maximum amplitude of the sloshing surface with respect to the equilibrium surface is less than 0.045 in subsection 6.5.

References

[1] Zhou J, Cai L, Feng J H and Xie W X 2007 *Appl. Math. Comput.* **186** 980

[2] He N Z, Wang N C, Shi B C and Guo Z L 2004 *Chin. Phys.* **13** 40

[3] Cheng X L, Hu F, Jiang J H, Li L and Ma X G 2006 *Chin. Phys.* **15** 149

[4] Chai Z H, Shi B C and Zheng L 2006 *Chin. Phys.* **15** 1855

[5] Xiong Y B and Wang H 2006 *Chin. Phys.* **15** 2352

[6] Brackbill J U, Kothe D and Zemach C 1992 *J. Comput. Phys.* **100** 335

[7] Olsson E and Kreiss G 2005 *J. Comput. Phys.* **210** 225

[8] Osher S and Sethian J A 1988 *J. Comput. Phys.* **79** 12

[9] Osher S and Fedkiw R P 2001 *J. Comput. Phys.* **169** 463

[10] Cai L, Feng J H, Xie W X and Zhou J 2006 *Appl. Numer. Math.* **56** 1555

[11] Xie W X, Cai L and Feng J H 2007 *Appl. Math. Model.* **31** 2503

[12] Harlow F H and Welch J E 1965 *Phys. Fluids* **8** 2182

[13] Jiang G S and Peng D 2000 *SIAM J. Sci. Comput.* **21** 2126

[14] Kurganov A and Levy D 2000 *SIAM J. Sci. Comput.* **22** 1461